Colloids and Surfaces A: Physicochemical and Engineering Aspects 668 (2023) 131439

Contents lists available at ScienceDirect

Colloids and Surfaces A: Physicochemical and Engineering Aspects

journal homepage: www.elsevier.com/locate/colsurfa

Triglyceride mixtures: Cold-bursting and double emulsion formation

Diana Cholakova, Desislava Glushkova, Martin Pantov, Slavka Tcholakova, Nikolai Denkov *

Department of Chemical and Pharmaceutical Engineering, Faculty of Chemistry and Pharmacy, Sofia University, 1 James Bourchier Avenue, 1164 Sofia, Bulgaria

GRAPHICAL ABSTRACT

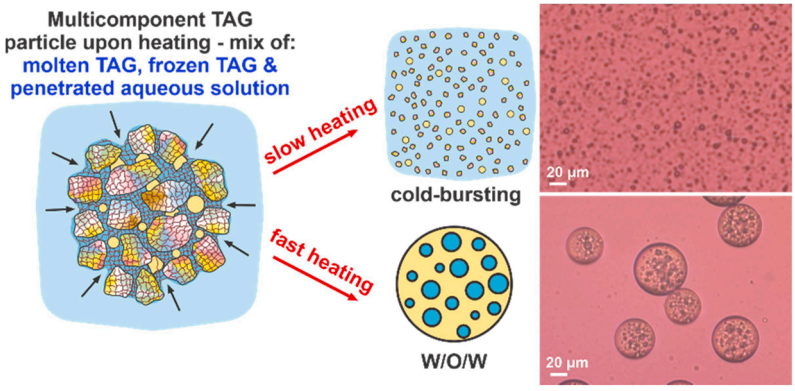

ARTICLE INFO

Keywords:
Fats
Polymorphism
Solid lipid nanoparticle
Double emulsion
Oil blend

ABSTRACT

It was shown recently that a solid-to-solid phase transitions (α-to-β, gel-to-crystal), typical for many lipid substances, can lead to formation of nanoporous network inside lipid micro-particles dispersed in aqueous surfactant solutions (Cholakova et al. *ACS Nano* **2020**, 14, 8594). These nanopores are spontaneously infused by the aqueous phase when appropriate combination of water-soluble and oil-soluble surfactants is applied. As a result, the initial lipid micro-particles can spontaneously burst into much smaller nanoparticles, just by cooling and heating of the initial dispersion. Under certain conditions, the infused aqueous phase is entrapped in the moment of lipid particle melting and double emulsion of type water-in-oil-in-water (W/O/W) is formed. The current study aims to clarify how the composition of the lipid micro-drops and surfactants affect the observed phenomena. Selected mixtures of monoacid triglycerides are studied systematically. The results show that the bursting efficiency usually decreases when the complexity of the lipid mixture increases, due to the expanded temperature interval for lipid melting. Nevertheless, complete particle bursting and lipid nanoparticles with diameters down to 20 nm are formed even for the most complex lipid compositions under appropriate conditions. The key mechanisms leading to efficient fragmentation and double emulsion formation are clarified, and the main governing factors are explored. On this basis, we reveal that the system behavior can be switched between complete particle bursting and W/O/W emulsion formation by: (1) Change in the cooling and heating rates without any changes in the chemical composition, (2) Change in the concentration of oil-soluble surfactant, and/or (3) Change in the phase in which the oil-soluble surfactant is introduced initially. Thus, we have formulated

* Correspondence to: Department of Chemical and Pharmaceutical Engineering, Sofia University, 1 James Bourchier Ave., Sofia 1164, Bulgaria.
E-mail address: nd@lcpe.uni-sofia.bg (N. Denkov).

https://doi.org/10.1016/j.colsurfa.2023.131439
Received 20 February 2023; Received in revised form 4 April 2023; Accepted 7 April 2023
Available online 10 April 2023

guiding rules to control the formation of lipid nanoparticles and W/O/W emulsions with triglyceride mixtures promising multiple potential applications.

1. Introduction

Triacylglycerides (TAGs) are chemical compounds composed of three fatty acids esterified to a glycerol. They are the most common type of fat in the human body and serve as a main energy source [1,2]. They are used in food supplements, pharmaceutics and cosmetics [3–5]. Triglyceride solid lipid nanoparticles (SLNs) have attracted distinctive interest recently, as they can encapsulate, protect and deliver lipophilic components such as flavors, vitamins, fragrances and bio-actives [6–8]. They are studied also in the context of targeted drug delivery and increased bioavailability in parenteral and oral medications [9,10]. However, their preparation is usually a challenge, because TAGs have low water solubility and relatively high interfacial tension and viscosity [11]. Thus, several consecutive cycles of high-pressure homogenization or sonication are applied usually to produce SLNs [12,13].

For the delivery of hydrophilic minerals, microelements, nutraceuticals, colorants and other useful components, double water-in-oil-in-water (W/O/W) emulsions are sometimes used. They provide several advantages over the simpler oil-in-water (O/W) emulsions as they contain encapsulated water droplets which are separated from the external continuous liquid medium by the lipid phase. For that reason, encapsulation in triglyceride W/O/W emulsions has been studied intensively in the last several years [14–22]. Double emulsions have been used also as vaccine adjuvants [23], drug delivery vehicles and for controlled release of actives [24–28]. In foods, W/O/W emulsions are investigated for their potential to replace partially the fats in low-fat products [29–32] and for preparation of products with reduced sodium content [33].

Double W/O/W emulsions are usually prepared *via* two-step emulsification procedure with mechanical stirring, ultrasound, high pressure homogenization and membrane emulsification [31], while microfluidic techniques offer procedures for single-step preparation [34,35]. However, a common problem in stabilization of such systems is the molecular transport of the encapsulated aqueous phase to the outer aqueous medium. Usage of solid (crystalline) lipid phase and/or crystallizable emulsifiers was shown to inhibit the molecular transport and to provide a longer shelf-life [20,28,36–39].

In our recent studies we demonstrated a novel route for preparation of triglyceride nanoparticles and double W/O/W triglyceride drops by applying one or several consecutive cycles of cooling and subsequent storage at low temperature or heating of lipid-in-water dispersions [40–42]. Solid lipid nanoparticles with sizes down to 20 nm were prepared by this "cold-bursting method" from an initial coarse emulsion, without any mechanical energy input. Using different combinations of TAGs and surfactants, double W/O/W emulsions were formed using similar temperature protocols [40].

The mechanisms of these phenomena involve polymorphic phase transitions of TAGs, see their schematic presentation in Fig. 1. The triglyceride molecules are known to arrange in three main polymorphs denoted as α, β' and β [43,44]. The thermodynamic stability, as well as the melting temperatures of the polymorphs increases from α to β. The molecules in the least stable α polymorph arrange in a hexagonal lattice with almost statistical orientation of the hydrophobic chains around their long axis, whereas orthorhombic and triclinic sub-cell structures are observed in β' and β polymorphs, respectively [43–45]. Upon rapid cooling, the triglyceride molecules usually arrange in the least stable α polymorph [46]. Afterwards, phase transition into the more stable β or β' phase is observed upon prolonged storage at low temperature or upon

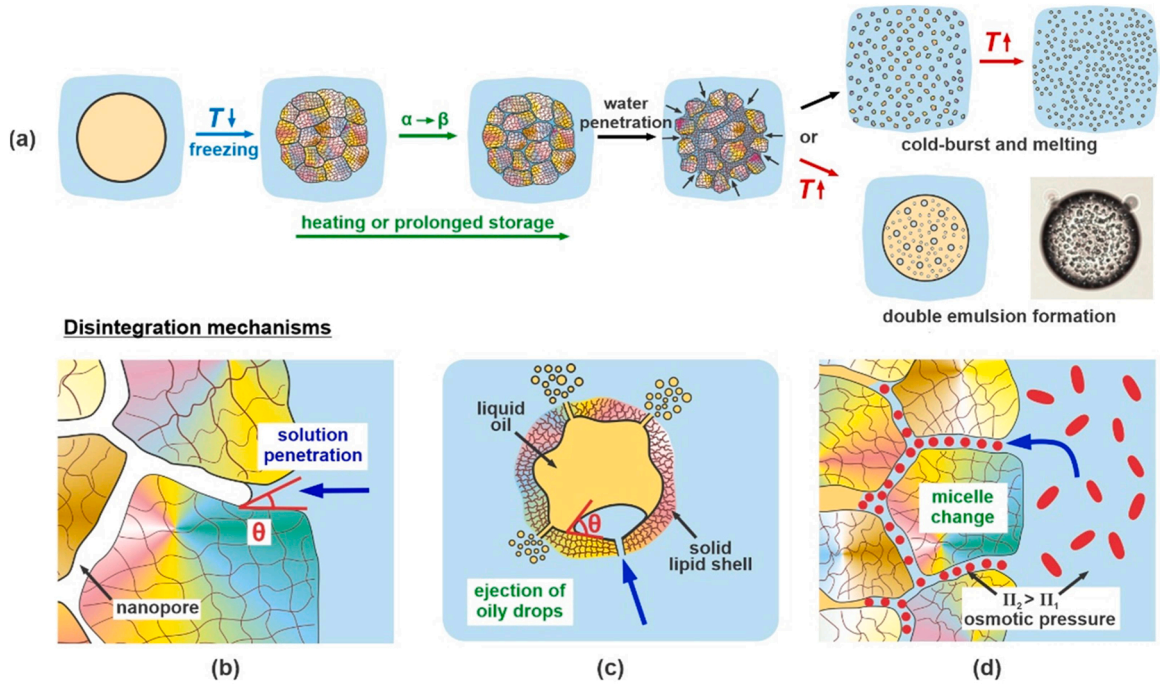

Fig. 1. Schematic presentation of the processes of cold-bursting and double emulsion formation. **(a)** TAG drops crystallize upon cooling in the unstable α polymorph. Upon prolonged storage or heating, α→β polymorphic transition occurs, leading to formation of nanoporous structure between the individual crystalline domains inside the frozen lipid particle. Afterwards, the aqueous phase penetrates into the nanopores between the domains, thus increasing the particle volume. Depending on the wetting properties of the aqueous solution, either particle disintegration is observed upon storage or heating, or double W/O/W emulsion is formed in the moment of TAG melting. **(b-d)** Schematics of the three different mechanisms identified to induce a spontaneous particle disintegration. See text for more details. Adapted from Refs. [40,41].

heating.

In our previous study, we showed that the aqueous surfactant solution infused the frozen triglyceride particles after the α-to-β phase transition, causing a significant increase of the particles volume (particle swelling), Fig. 1a,b [40]. This process was explained with the formation of inner nanoporous structure in the lipid phase after its α-to-β phase transition, due to the higher mass density of the β-polymorph and the related crystal domains' shrinkage upon this transition [40,43,47]. As a result of the nanopore infusion by aqueous surfactant solution, spontaneous disintegration of the initial lipid micro-particle into much smaller nanoparticles was observed for emulsions, stabilized by surfactants which wet well the surface of the lipid domains – the three-phase contact angle at the air-triglyceride-water interface was lower than *ca.* 30° in these emulsions. The particle disintegration was observed at temperatures below that of TAG melting. Therefore, this method of nanoparticle formation was termed "cold-bursting". By contrast, when the wetting properties of the surfactant solutions were poor and the systems exhibited higher contact angles (≈ 100° or higher) we observed the formation of double W/O/W emulsions in the moment of TAG melting [40].

The cold-bursting process was originally observed with pure triglycerides, alkanes, diglycerides, phospholipids [40] and more recently with natural triglyceride oils, *e.g.* coconut oil, lard and cocoa butter [41]. In [41] we showed that the good wetting ability of the surfactant solution is insufficient for efficient disintegration of lipid particles containing complex triglyceride mixtures, *e.g.* with mixed fatty acid residues. The main difference between the pure monoacid triglycerides and the natural triglyceride oils and fats is the temperature interval for their melting. The pure substances exhibit a relatively sharp melting peak in a narrow temperature interval of a few degrees, whereas the melting process in natural triglyceride oils and fats can span over 10–20 °C or even more. Therefore, to efficiently decrease the particle size in emulsions of natural TAGs, the cold-bursting process should be operative when liquid and solid domains coexist [41].

Our experiments showed that such high efficiency could be achieved by two complementary mechanisms. When the surfactant solution was able to de-wet the molten oil from the still frozen lipid domains (*i.e.* the three-phase contact angle "surfactant solution-liquid oil-solid lipid substrate" measured through the surfactant solution was relatively small), we observed the ejection of small liquid oily drops from the still solid lipid shell prior to its melting, Fig. 1c. Very efficient drop disintegration was observed also by creation of osmotic pressure difference between the penetrating aqueous phase and the continuous aqueous medium outside the lipid particle. Such osmotic pressure appeared when the surfactant solution used for emulsion stabilization contained relatively large supramolecular aggregates, such as very large cylindrical micelles or micellar aggregates, Fig. 1d [41]. Turbid aqueous solutions were prepared by mixing water-soluble and oil-soluble surfactants in appropriate ratios – these aqueous solutions contained supramolecular aggregates which scattered intensively the visible light. When such surfactant solutions infused the nanopores in the lipid particle, the oil-soluble surfactant adsorbed on the lipid surface of the nanopores. As a result, the size of the penetrated micelles decreased, while their number increased. The number density difference of the aggregates inside (in the nanopores) and outside (in the continuous phase) created a difference in the osmotic pressure which enhanced the influx of water, thus boosting the cold-bursting efficiency. Similar effect, which enhanced the cold-bursting efficiency, was observed when we dissolved salt in the continuous phase [42].

In the current study we investigate systematically oil-in-water emulsions prepared with pre-mixed pure monoacid TAGs. The major aim is to clarify how the composition of the TAG mixture affects the processes of cold-bursting and double emulsion formation. Comparison is also made between the pure monoacid TAGs, their mixtures and natural TAG-based oils and fats. We clarified further the role of the oil-soluble surfactant and explained for the first time why the oil-soluble surfactant needs to be present when the TAG particles crystallize to achieve best cold-bursting efficiency. Based on this understanding, we learned how to switch systems' behavior between efficient cold-bursting and efficient double W/O/W emulsion formation, by changing the temperature protocol only. These findings complete our understanding and provide powerful guidelines for optimization and control of these phenomena with potential multiple applications in pharmaceutics, cosmetics, food industry and chemical technologies.

The paper is organized as follows: Section 2 presents the materials and experimental methods. The experimental results and discussion in Section 3 are presented in three sub-sections: first we discuss the role of TAG mixture composition; then we explain the role of the oil-soluble surfactant type; finally, we discuss the factors that can be used to control the processes of cold-bursting and double emulsion formation. Section 4 summarizes the main conclusions.

2. Materials & methods

2.1. Materials

We study O/W emulsions, subjected to cycles of subsequent cooling and heating. As a dispersed phase we use in-house prepared mixtures of monoacid saturated triglycerides (TAGs) with different chain lengths, ranging from C_8 (tricaprylin) to C_{18} (triolein). Tricaprin (purity > 98%), trilaurin (> 98%) and trimyristin (> 95%) were purchased from TCI Chemicals, whereas tricaprylin (purity ≥ 97%), tripalmitin (≥ 85%) and triolein (≈ 65%) were products of Sigma-Aldrich. All triglycerides were used as received.

The studied TAG mixtures, see Table 1, were prepared by weighting the necessary amount of each TAG. These mixtures were homogenized by melting at 70 °C for 30 min, under mild stirring. The mixtures are denoted as M*X*, where the number "*X*" shows the number of components in the mixture and it varies between 2 and 6. An additional letter (*a* or *b*) is added after *X* when more than one mixture with the same number of mixed triglycerides (at different ratios) is included in the study. The studied mixtures were designed so that the total fatty acid composition of the most complex mixture with 6 components resembles that of the natural coconut oil (CNO). The simpler mixtures consecutively excluded the TAGs with lower concentrations in CNO. We note that, although the total fatty acid composition of our mixtures resembles that of the natural CNO, their properties remain distinctly different because *ca.* 80% of the TAG molecules in CNO contain mixed-chain TAGs, whereas our mixtures contain monoacid TAG molecules [41,48].

The initially prepared TAG-in-water emulsions were stabilized by water-soluble and oil-soluble surfactants. Polyoxyethylene glycol sorbitan monolaurate ($C_{12}SorbEO_{20}$, trade name Tween 20, purchased by Sigma-Aldrich) with concentration of 1.5 wt% was applied as water-soluble surfactant in most experiments. This surfactant is widely used in many food, pharmaceutical and cosmetic products [49–52]. We used also the water-soluble polyoxyethylene (20) stearyl ether, *i.e.* $C_{18}EO_{20}$, trade name Brij S20 (Sigma-Aldrich).

The oil-soluble surfactants included monoglycerides (MG) with different chain lengths: monocaprin (C_{10}MG, 1-decanoyl-*rac*-glycerol, product of Sigma-Aldrich, purity ≥ 99%), monopalmitin (C_{16}MG, TCI

Table 1
Composition of the model mixtures and notation used throughout the text.

Triglycerides notation		Monoacid triglyceride content in the model mixtures, wt%						
		M2a	***M2b***	***M3***	***M4***	***M5a***	***M5b***	***M6***
C_8TAG	CaCaCa					7		7
C_{10}TAG	CCC				9	15	15	8
C_{12}TAG	LLL	50	70	60	60	50	50	50
C_{14}TAG	MMM	50	30	25	20	18	18	18
C_{16}TAG	PPP			15	11	10	10	10
$C_{18:1}$TAG	OOO						7	7

Chemicals, > 95%), monostearin (C_{18}MG, TCI Chemicals, > 60%), monoolein ($C_{18:1}$MG, 1-oleoyl-*rac*-glycerol, product of Sigma-Aldrich, purity ≥ 99%), and commercial monoglyceride mixture containing C_{16}MG:C_{18}MG:$C_{18:1}$MG = 55:40:5 (denoted as C_{16-18}MG). In most experiments, the oil-soluble surfactants were added into the aqueous phase (see Section 3.3.2 for more detailed explanations). All surfactants were used as received.

All aqueous solutions were prepared using deionized water with resistivity > 18 MΩ·cm, purified by Elix 3 module (Millipore).

For hydrophobization of the glass substrates used for three-phase contact angle measurements we used hexamethyldisilazane (HMDS), product of Sigma-Aldrich.

2.2. Methods

2.2.1. Emulsion preparation

Emulsions were prepared using either rotor-stator homogenizer Ultra-Turrax T25 (IKA-Werke GmbH & Co. KG, Germany) for fast screening of sample behavior, or membrane emulsification (SPG, Japan) to produce monodisperse droplets in the systematic experiments, see Refs. [41,53] for more detailed explanations of the emulsification procedures.

2.2.2. Optical observations upon cooling and heating

The emulsion behavior upon thermal cycling was studied with emulsion samples placed in glass capillaries with rectangular cross section (100 μm height, 1 or 2 mm width), which were enclosed inside a custom-made thermostatic chamber connected to a thermostat. The samples were observed with an optical microscope AxioImager.M2m in transmitted cross-polarized light with included compensator λ-plate, situated at 45° after the polarizer and before the analyzer [40,41,53]. The sample temperature was monitored with calibrated thermo-couple probe, as explained earlier [40,41,53].

Four main cooling-heating protocols were applied, combining *rapid* or *slow* cooling and *fast* or *slow* heating. We denote by "*rapid cooling*" experiments in which the pre-heated sample containing molten lipid particles ($T \approx 60$ °C) was inserted into a pre-cooled thermostatic chamber, $T \approx 0$ °C, thus achieving a cooling rate ≈ 25 °C/s. In other experiments, we applied also *slow* cooling with controlled rate ≈ 1 °C/min. The heating step was performed with *low rate* ≈ 1 °C/min or with *fast heating* (rate ≈ 5 °C/min).

2.2.3. Three-phase contact angle measurements

The wetting properties of surfactant solution drops, placed on various solid MG or TAG substrates, were also studied. The substrates were prepared by placing a small molten amount of the studied MG/TAG mixture over a pre-hydrophobized glass. The molten lipid was then covered with a second pre-hydrophobized glass to obtain a layer with homogeneous thickness. The temperature of the glass slides was fixed between 12 and 23 °C for TAG substrates depending on the mixture composition, to ensure quick crystallization of the lipid phase and it was equal to 57 °C when monoglyceride substrates were prepared. The three-phase contact angle measurements were performed at a fixed temperature of 25 °C using DSA 100E apparatus, Kruss, Germany. For these experiments, a small drop of the surfactant solution was placed over the studied TAG substrate and the shape of the surfactant drop was monitored for a period of 10 min. The contact angles were measured using the build-in software in the DSA instrument.

2.2.4. Differential scanning calorimetry (DSC)

The thermal behavior of some of the studied TAGs and their mixtures was investigated using apparatus DSC 250, TA Instruments, USA. The samples were melted, measured in TZero pans and hermetically sealed with TZero lids. The cooling was performed with 1 or 20 °C/min rate, while the heating rate was fixed at 1 °C/min. The obtained thermograms were analyzed with TRIOS data analysis software, TA Instruments.

2.2.5. Small-and wide-angle X-ray scattering (SWAXS)

The structural changes occurring upon cooling and heating in some of the emulsions and bulk TAGs were studied with Xeuss 3.0 equipment, Xenocs, France. The samples for these experiments were placed in cylindrical borosilicate glass capillary tubes with outer diameter of 1 mm, products of Capillary Tube Supplies Ltd. Cu K-α radiation with wavelength of λ ≈ 1.54 Å was used and the scattered signal was detected with an EIGER2 R 4 M detector at a sample-to-detector distance of 286 mm. Exposure time for a single image was 30–90 s. HFSX350 high temperature stage, equipped with T96 temperature controller and LNP96 liquid nitrogen pump, all products of Linkam Scientific Instruments Ltd., UK, were used for precise temperature control in the samples.

2.2.6. Cryo-TEM imaging

The lipid nanoparticles prepared after few consecutive thermal cycles were observed using cryo-TEM. Vitrobot system (FEI, USA) was used for specimen preparation at 25 °C and 100% relative humidity. Briefly, a drop of the tested emulsion sample was placed on a holey carbon copper TEM grid, the excess liquid was blotted off with filter paper and then the sample was plunged into a liquid propane-ethane mixture to form a vitrified specimen. Afterwards, the specimen was transferred into a liquid nitrogen and stored in it until further inspection.

The cryo-TEM imaging was performed using Gatan cryo-specimen holder at JEM2100, JEOL high-resolution transmission electron microscope. An acceleration voltage of 200 kV was used. Micrographs were recorded with Gatan Orius SC1000 camera.

3. Results and discussion

3.1. Role of TAG mixture composition for the cold-bursting process

In this section we describe the results obtained with various emulsified TAG mixtures upon *rapid cooling* (≈ 25 °C/s) and subsequent *slow heating* (≈ 1 °C/min). Results obtained with emulsions, in which the aqueous phase contains 1.5 wt% $C_{12}SorbEO_{20}$ + 0.5 wt% $C_{18:1}EO_2$, are presented in Fig. 2a-h and Supplementary Movies 1 and 2. As seen from the microscopy images, the cold-bursting process with mixed TAG particles becomes less efficient when the mixtures become more complex in composition. Complete disintegration of the frozen TAG particles into numerous droplets with size ≈ 1 μm or smaller is observed for *M2* TAG mixtures (LLL+MMM). Significant cold-bursting and drop size decrease is also observed in the three-, four- and five-component mixtures; however, the obtained drops are with micrometer diameters. Very limited disintegration is observed for the particles containing *M6* mixture. In this system, a small number of droplets detach from the surface of the original TAG particle upon heating. No disintegration is observed when the same temperature protocol is applied to CNO dispersions in the same surfactant solution, Fig. 2i.

In our previous study we described the cold-bursting process with TAG particles of pure triglycerides [40]. We showed that the emulsion behavior upon heating (cold-bursting *vs* double emulsion formation) is strongly affected by the three-phase contact angle at the surfactant solution-TAG-air interface (TAG serves as a solid substrate in these measurements) [40]. To check whether the decreased bursting efficiency in complex triglyceride mixtures is due to changes in the contact angles, we prepared solid TAG substrates in the most stable β polymorph and measured the contact angles as described in section *Methods*. If the three-phase contact angle is higher for mixed TAG substrates, one could explain the decreased bursting efficiency in the emulsions containing complex TAG mixtures.

The results for the three-phase contact angles are presented in Fig. 3. Surprisingly, instead of the expected three-phase contact angle increase for the more complex mixtures, the experiments showed the opposite trend. The contact angle, measured 10 s after a drop of 1.5 wt% $C_{12}SorbEO_{20}$ solution (without oil-soluble surfactant added) was placed on the substrate, was *ca.* 68 ± 6° for pure trimyristin substrate and

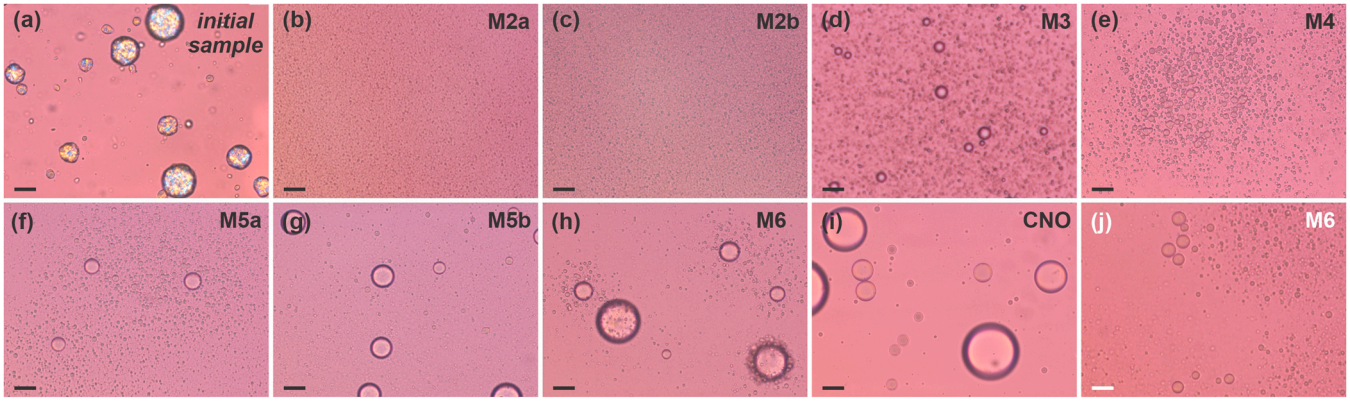

Fig. 2. Optical microscopy images illustrating the dependence of cold-bursting efficiency on the triglyceride mixture content. Rapid cooling with rate of ≈ 25 °C/s was applied for all samples shown in this figure. **(a)** Representative image for the emulsion samples with frozen particles, prior to their heating. The initial drop diameter is $d_{32} \approx 20 \pm 5$ μm. **(b-j)** Images showing the various samples studied after their heating. **(b-i)** The oily drops (oil composition is denoted on the images, see also Table 1) are dispersed in 1.5 wt% $C_{12}SorbEO_{20}$ + 0.5 wt% $C_{18:1}EO_2$ surfactant solutions. Heating rate ≈ 1 °C/min, except for CNO where the rate is 0.5 °C/min. **(j)** Drops composed of *M6* mixture dispersed in 1.5 wt% $C_{12}SorbEO_{20}$ + 0.5 wt% $C_{18:1}MG$ and heated with rate of 4.2 °C/min. Note that the cold-bursting efficiency for the latter surfactant solution is much higher, compared to the solution of $C_{12}SorbEO_{20}$ + $C_{18:1}EO_2$ shown in (h), even when faster heating is used. The cold-bursting efficiency for this sample increases at lower heating rates and becomes comparable to that shown in (e), see Supplementary Movie 1. Scale bars = 20 μm.

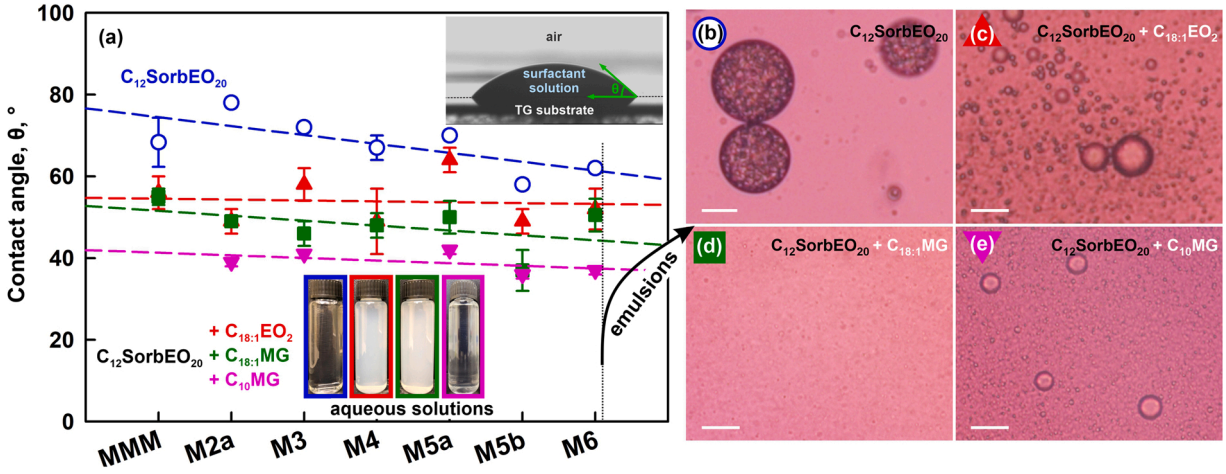

Fig. 3. Three-phase contact angles and optical microscopy images. **(a)** Dependence of three-phase contact angle on the composition of the TAG mixture for several surfactant solutions. Empty blue circles are for solution of 1.5 wt% $C_{12}SorbEO_{20}$ without oil-soluble surfactant; full symbols are for 1.5 wt% $C_{12}SorbEO_{20}$ combined with 0.5 wt% oil-soluble surfactant: red – $C_{18:1}EO_2$; green – $C_{18:1}MG$, and pink – $C_{10}MG$. The composition of TAG mixtures is presented in Table 1. Inset: pictures of bottles filled with the aqueous surfactant solutions (no added oil, $T = 25$ °C). Note that the solutions of $C_{12}SorbEO_{20}$ (b) and $C_{12}SorbEO_{20}$ + $C_{10}MG$ (e) are transparent, whereas $C_{12}SorbEO_{20}$ + $C_{18:1}EO_2$ (c) or + $C_{18:1}MG$ (d) are turbid. **(b-e)** Optical microscopy images obtained after *rapid cooling* and subsequent *slow heating* of the emulsion of *M6* mixture, dispersed in different surfactant solutions, as denoted on the images. Scale bars = 20 μm.

decreased slightly to 60 ± 2° for *M5b* and *M6* substrates. The average angle measured for the aqueous solution containing oil-soluble surfactant, $C_{12}SorbEO_{20}$ + $C_{18:1}EO_2$, was slightly lower ≈ 55 ± 6° and did not depend significantly on the specific composition of the TAG substrate, see the red circles in Fig. 3a. Therefore, the decreased bursting efficiency with more complex TAG mixtures cannot be explained with changes in the three-phase contact angles.

A major difference between the pure individual TAGs and TAG mixtures, regardless of whether they contain monoacid fatty acid residues (as the model mixtures in the current study), or contain different chains in the same TAG molecule (as the natural oils and fats), is the temperature interval in which they melt. Pure monoacid triglycerides melt in a narrow temperature interval, whereas the same interval for natural TAG oils is much wider, *ca.* 20 °C [41]. In a previous study, exploring the behavior of monoacid TAG mixtures, we showed that the melting of such mixtures is governed mostly by the melting temperatures of the individual TAG species included in the mixtures [54]. Therefore, the increase in the number of components in the mixture leads to a significant increase of the temperature interval for mixture melting, *i.e.* for coexistence of already melted (fluid) and still frozen solid domains. The comparison between the DSC signals, obtained with different mixtures, shows that this interval increases from 15 °C for *M2a* to 20 °C for *M4*, and to 29 °C for *M6*, see Supplementary Figure S1.

We can conclude that the coexistence of molten and solid domains upon heating suppresses the TAG particle disintegration in ($C_{12}SorbEO_{20}$ + $C_{18:1}EO_2$) solution in the emulsions containing complex TAG mixtures when compared to pure TAGs, under otherwise equivalent conditions (same surfactants, cooling and heating rates, particle sizes). The three-phase contact angles were found to depend mainly on the surfactants added, whereas the effect of the TAG mixture composition was minor.

Next, we performed experiments with different oil-soluble surfactants to reveal their role and to check whether the bursting efficiency can be improved for the complex TAG mixtures.

3.2. Role of surfactant type in the cold-bursting process

Besides $C_{18:1}EO_2$ surfactant, we studied several other oil-soluble surfactants for comparison, see *Materials* section. Monoolein ($C_{18:1}MG$) was chosen, because it has the same hydrophobic chain as $C_{18:1}EO_2$ surfactant with different hydrophilic head-group. We studied also a shorter monoglyceride, monocaprin ($C_{10}MG$). These two surfactants were chosen, based on our previous results with CNO emulsions, in which we showed that these surfactants are more efficient for cold-bursting of CNO drops [41]. In all cases, $C_{12}SorbEO_{20}$ surfactant was also present in the aqueous solutions to stabilize the TAG-in-water emulsions and to ensure, at least partial solubilization of the oil-soluble surfactant in the $C_{12}SorbEO_{20}$ micelles.

3.2.1. Role of three-phase contact angle

First, we performed three-phase contact angle measurements with the various surfactant solutions, see the green and purple symbols in Fig. 3a. The lowest values of the three-phase contact angles, $\approx 41 \pm 2°$, were measured with $C_{12}SorbEO_{20} + C_{10}MG$ combination. No dependence on TAG mixture composition was observed for this surfactant solution. The three-phase contact angles for $C_{12}SorbEO_{20} + C_{18:1}MG$ were slightly higher and similar to those measured with $C_{12}SorbEO_{20} + C_{18:1}EO_2$.

To check whether the smaller three-phase contact angle for $C_{12}SorbEO_{20} + C_{10}MG$ solution leads to better particle disintegration, we performed experiments with *M6* particles, dispersed in this surfactant solution. The image shown in Fig. 3e is obtained after *slow heating* of *rapidly cooled* emulsion drops in this system. The disintegration efficiency was slightly improved, but similar to that observed in $C_{12}SorbEO_{20} + C_{18:1}EO_2$ solution, *viz.* many drops with size bigger than 10 μm remained in the sample after heating, compare Figs. 3c and 3e. In contrast, when the same experiment was performed with $C_{12}SorbEO_{20} + C_{18:1}MG$ solution, we observed complete particle disintegration and sub-micrometer drop formation, see Fig. 3d and Supplementary Movie 3. Therefore, we cannot explain the significantly different bursting efficiency in the surfactant solutions with the same water soluble-surfactant and different oil-soluble surfactants by considering the three-phase contact angles only. Another explanation should be found for the effect of the various surfactant mixtures studied.

3.2.2. Supramolecular aggregates in the solution

Combination of water-soluble and oil-soluble surfactant in the aqueous phase is used for two main reasons. First, the addition of oil-soluble surfactant decreases further the three-phase contact angle, leading to better wetting of the triglyceride substrate by the surfactant solution, see Fig. 3a. Second, we showed in our previous study that the presence of supramolecular structures and/or non-spherical micelles in the aqueous phase may lead to an additional osmotic effect which boosts significantly the cold-bursting process [41]. Once the aqueous surfactant solution penetrates the nanopore network inside the lipid particles, the supramolecular aggregates release part of the oil-soluble surfactant molecules (which adsorb on the particle surface) and the micelles become enriched in water-soluble surfactant. This change in composition induces micelle break-up into smaller (spherical) and more numerous micelles, see Fig. 1d. As a result, the micelles inside the nanopores create an osmotic pressure gradient, causing an enhanced influx of water into the nanopores.

The formation of non-spherical micelles and supramolecular aggregates in the aqueous solution depends on the packing of the oil-soluble and water-soluble surfactant molecules. It can be assessed qualitatively by comparing the turbidity of the aqueous solutions. The solutions of $C_{12}SorbEO_{20} + C_{18:1}EO_2$ and $C_{12}SorbEO_{20} + C_{18:1}MG$ are turbid and look similarly in the entire temperature interval relevant for the experiments, between 5 °C and 60 °C. In contrast, the inclusion of shorter $C_{10}MG$ molecules into mixed aggregates with $C_{12}SorbEO_{20}$ leads to almost transparent solution of these two surfactants, see inset in Fig. 3a. Thus, we deduce that the lower bursting efficiency of *M6* particles in $C_{12}SorbEO_{20} + C_{10}MG$ solution is caused by the suppressed osmotic pressure effects. Similar results were obtained with *M6* drops dispersed in $C_{18}EO_{20} + C_{12}EO_4$ surfactant solution, which is also transparent, see Supplementary Figure S2. However, the osmotic pressure does not explain the different performance of $C_{12}SorbEO_{20}$ solutions in the presence of the two oil-soluble surfactants with oleic tails – both solutions contain supramolecular aggregates (see inset in Fig. 3a) and have similar three-phase contact angles on TAG substrates, while exhibiting very different cold-bursting efficiency. Therefore, some additional effect should be invoked to explain the boosting effect of $C_{18:1}MG$ and $C_{18:1}EO_2$ oil-soluble surfactants.

3.2.3. TAG-emulsifier crystallization

Another possible explanation for the observed differences could be that the oil-soluble surfactants influence the TAG crystallization in the emulsion drops upon cooling. For example, saturated monoglycerides are known to affect the crystallization of TAGs and can act as nucleation seeds [55–57].

To explore this possible explanation, we performed SWAXS experiments with emulsified drops, dispersed in the surfactant solutions of $C_{12}SorbEO_{20} + C_{18:1}MG$ or $C_{12}SorbEO_{20} + C_{18:1}EO_2$ for comparison. The sample behavior was very similar, without any significant differences, see Supplementary Figure S3. However, if structural differences occur on the drops' surface or in a small fraction of the crystalline domains only, they can be missed in SWAXS experiments, due to insufficient intensity of the respective signal. In previous experiments with emulsions, we showed that phase with thickness 5–10 nm, which forms on the drops surface and is detected by DSC experiments, cannot be detected in SAXS spectra even when synchrotron radiation source is used [53,58]. Formation of thicker phases was needed to see a small peak in the scattered X-ray signal [58].

Therefore, we performed DSC and SWAXS measurements with the bulk *M6* mixture in the presence and in the absence of oil-soluble surfactants to check how these surfactants affect the phase behavior of the TAG mixtures, see Fig. 4 and Supplementary Figure S4. The melting enthalpy for *M6* sample in the absence of surfactant was 140 ± 4 J/g. In the presence of 10 wt% $C_{18:1}MG$ this enthalpy decreased to 127 ± 4 J/g, whereas in the presence of 10 wt% $C_{18:1}EO_2$ it was $\approx$ 136 ± 1 J/g. Note that the enthalpy for *M6* + $C_{18:1}MG$ mixture is equal to 90% of the enthalpy for pure *M6* mixture, *i.e.* $C_{18:1}MG$ either does not crystallize in the presence of the TAGs and does not contribute to the measured enthalpy, or it decreases the ordering of TAG molecules again resulting in decreased enthalpy. In contrast, the ethoxylated oleyl alcohol surfactant $C_{18:1}EO_2$ should crystallize with the TAG mixture, as it contributes to the measured melting enthalpy.

The structural data obtained from SWAXS experiments confirmed these conclusions, see Fig. 4. Both oleyl-containing surfactants were found to co-crystallize with the TAG mixture in the less stable α and β' polymorphs. However, once the phase transition into the most stable β phase began, the $C_{18:1}MG$ surfactant phase-separated from the TAG mixture, forming a distinct phase with larger interlamellar spacing of $\approx$ 4.83 nm. No such phase was observed with *M6* sample in the absence of surfactant (see Supplementary Figure S4a) or in the presence of $C_{18:1}EO_2$ surfactant, see Fig. 4b,c. The other main peaks observed in the SAXS spectra were identical to those observed without surfactant added, see Fig. 4c and Supplementary Figure S4a. Similar phase separation in presence of $C_{18:1}MG$ was observed also with the binary TAG mixture *M2a*, see Supplementary Figure S5.

These results evidence that the main difference between $C_{18:1}EO_2$ and $C_{18:1}MG$ surfactants is that $C_{18:1}EO_2$ co-crystallizes with TAG mixture and does not change its structure, whereas $C_{18:1}MG$ forms separate domains. Hence, the increased bursting efficiency in the presence of $C_{18:1}MG$ can be explained as follows: this surfactant transfers from the surfactant supramolecular aggregates into the triglyceride oily phase after emulsion formation (when the TAG drops are still in liquid

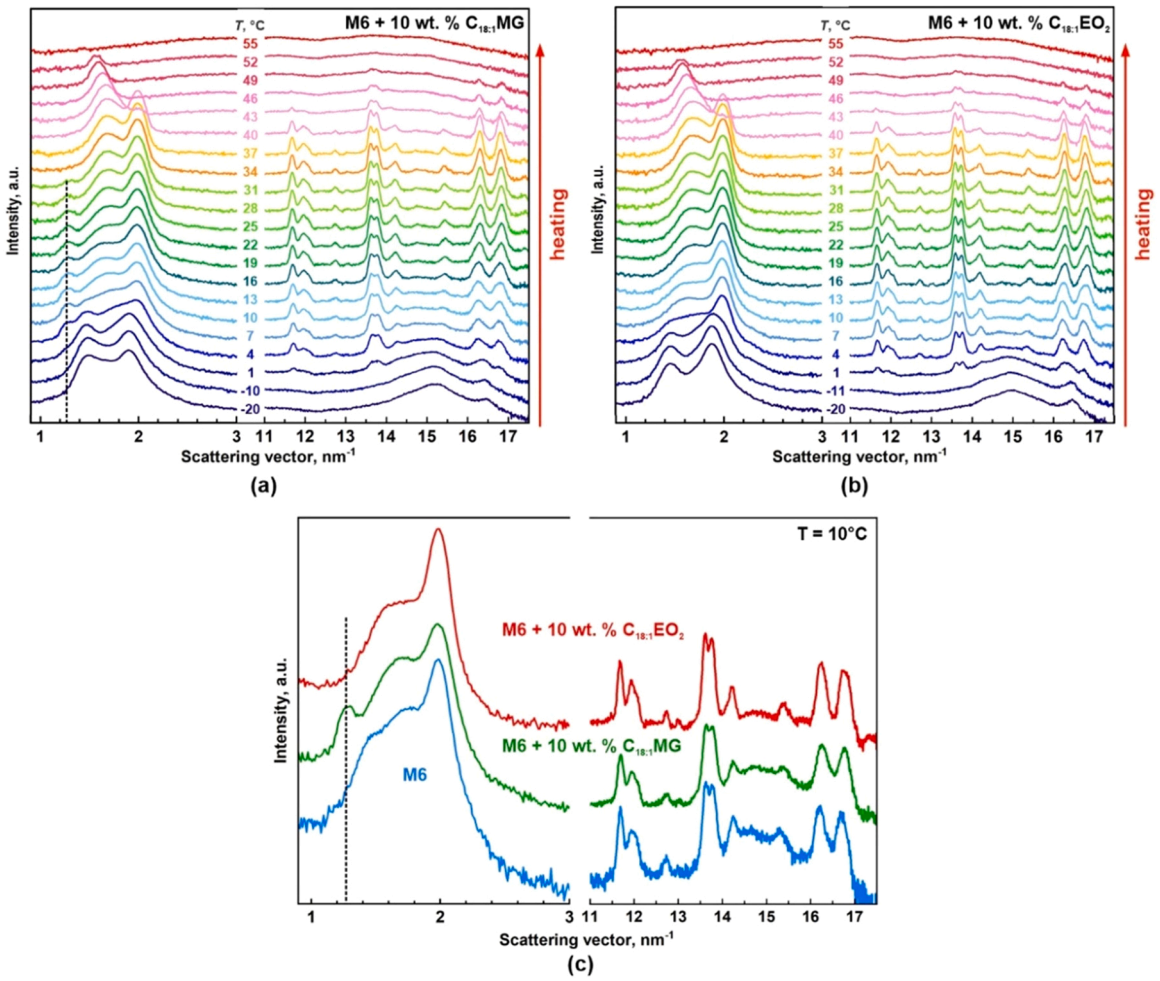

Fig. 4. SAXS and WAXS spectra obtained upon 1 °C/min heating of bulk *M6* + 10 wt% oil-soluble surfactant. These samples had been rapidly pre-cooled to −20 °C. (a) *M6* + $C_{18:1}$MG and (b) *M6* + $C_{18:1}EO_2$. The polymorphic phase transition to the most stable β phase begins at $T \approx 1$ °C. Note that $C_{18:1}$MG phase separates from the TAG mixture upon β phase formation (see the peak at $q \approx 1.3$ nm^{-1}, showed with dashed line in (a), whereas no such peak is observed with $C_{18:1}EO_2$ surfactant. The other main peaks, showing the TAG crystallization, are equivalent in the two samples. (c) Comparison between the spectra obtained at 10 °C for *M6* (blue curve), *M6* + 10 wt% $C_{18:1}$MG (green curve) and *M6* + 10 wt% $C_{18:1}EO_2$ (red curve).

state); upon cooling, $C_{18:1}$MG forms separate crystalline domains that melt at $T \approx 34$ °C, expanding the inner nanoporous structure and facilitating the water influx. These latter effects are missing in the presence of $C_{18:1}EO_2$ surfactant, which co-crystallizes with the TAG molecules. The explained mechanisms are illustrated in Fig. 5.

We note that similar phase separation of mono- and diglycerides

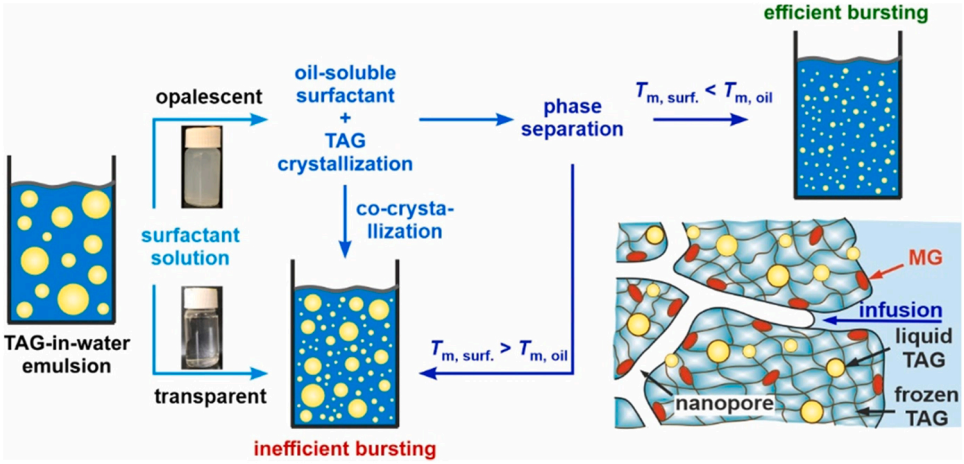

Fig. 5. Schematic presentation of the requirements for efficient bursting with complex TAG mixtures. The initial surfactant solution should contain both oil-soluble and water-soluble surfactants. The most efficient bursting upon cooling and heating is observed when the osmotic pressure effect is present, the oil-soluble surfactant crystallizes separately from the TAG domains and it melts at lower temperature than the TAG mixture.

from crystallizing TAG mixtures (75 wt% coconut oil + 25 wt% sunflower oil) was reported in Ref. [59]. These authors showed that mono-diglyceride mixture (with saturated 16-carbon chains) melted and crystallized independently of the fat blend, whereas Tween 80 surfactant (polyoxyethylene(20) sorbitan monooleate) led to the formation of less ordered TAG crystals, without phase separating from them.

To further elucidate the effect of monoglycerides on TAG crystallization and on the related cold-bursting process, we performed experiments with *M6* + 10 wt% C_{16}MG, *M6* + 10 wt% C_{18}MG and *M6* + 10 wt % $C_{16–18}$MG systems. The structural data showed that monopalmitin, monostearin and their mixture crystallized separately from the TAG domains, see Supplementary Figure S4c-e. These monoglycerides have saturated chains and they melt at higher temperatures compared to the TAG mixtures. The experiments with emulsions prepared with C_{12}SorbEO$_{20}$ and various saturated monoglycerides dispersed in the aqueous phase showed that these MGs also enhance the bursting process when compared to that observed in the absence of oil-soluble surfactants, see Supplementary Figure S6. However, the bursting efficience remained lower when compared to that observed with monoolein ($C_{18:1}$MG) which phase separates from the TAGs and melts at lower temperatures.

To explain the effect of the saturated MGs, we hypothesized that once the MG phase separates from the TAG, it forms more hydrophilic domains (hydrophilic "patches" on the nanopore surface) which enhance the aqueous phase infusion and the respective cold-bursting efficiency. We tested this hypothesis by measuring the three-phase contact angles of aqueous solution drop, placed over solid MG substrates. Indeed, the measured angles were significantly lower compared to those observed with TAG substrates – the average three-phase contact angle for C_{12}SorbEO$_{20}$ ± $C_{18:1}$MG drop placed over frozen C_{16}MG or C_{18}MG was ≈ 18 ± 3° when measured about 10 s after the drop was deposited over the substrate and it decreased down to ≈ 0° after a few minutes. In comparison, when the same experiments were performed with MMM substrate, the angle was higher than 50° and remained almost constant for more than 5 min, see Fig. 3a. Therefore, the primary effect of the MG phase separation is to form hydrophilic patches in the nanoporous structure which boost the aqueous phase infusion. When MG melts before the TAGs, the pores probably swell and the cold-bursting efficiency is additionally improved.

Finally, to prove that the presence of oil-soluble surfactant inside the crystallized TAG structure is of major importance, we prepared *M6* emulsion, stabilized by C_{12}SorbEO$_{20}$ surfactant only (without oil-soluble surfactant) and froze the *M6* drops rapidly. In this way, we were sure that the obtained crystalline TAG structure was not affected by oil-soluble surfactants. Afterwards, we transferred these frozen *M6* particles into a solution of C_{12}SorbEO$_{20}$ + $C_{18:1}$MG and then heated them under an optical microscope, see Supplementary Figure S7. As seen from the microscopy images, the efficiency of disintegration was much worse compared to that observed with drops which were crystallized in presence of $C_{18:1}$MG surfactant (Fig. 3d). Therefore, the presence of oil-soluble surfactant in the moment of crystallization has a major impact on the subsequent particle bursting upon heating, which is explained with the more hydrophilic domains which form upon MG phase separation from the TAGs.

In conclusion, very efficient particle disintegration is possible even for the most complex TAG mixtures studied which contained up to six TAG species. The main requirement is that the aqueous solution, in which the particles are dispersed, contains large supramolecular surfactant aggregates. An osmotic pressure gradient arises once these aggregates infuse the particles and release part of the oil-soluble surfactant molecules. Additionally, the cold-bursting efficiency is boosted if the oil-soluble surfactant is able to phase separate from the crystallized TAG molecules and melts at lower temperature compared to TAG. In the latter case, the size of the inner nanoporous structure is increased, thus improving the cold-bursting efficiency.

Experiments were performed also with oil-soluble surfactant which had been dissolved initially in the oily phase – the respective results are presented in Section 3.3.2 and will be compared to the results described above.

3.3. Cold-bursting vs double emulsion formation

In this section we summarize the effects of all main experimental factors affecting the observed processes for given composition of the lipid and surfactant mixtures. First, we show how the peculiar phase behavior of mixed TAGs can be used for controlled switch between complete particle cold-bursting and double emulsion formation by changing the cooling and heating rates only, without any change in the sample composition. Then, we discuss the role of the oil-soluble surfactant concentration when it is dispersed in the aqueous phase. Next, we show that double W/O/W emulsions are formed for all temperature protocols when the oil-soluble surfactant is pre-dissolved in the oily phase, *viz.* it is missing in the aqueous phase. Finally, we discuss the effect of the initial drop size.

3.3.1. Temperature protocol

The applied thermal cycles include two steps: cooling and heating. The effect of cooling rate is easily understood, considering the available time for molecular rearrangement and the related size of the formed crystalline domains. Upon higher cooling rates, smaller crystal domains are formed and *vice versa* [46]. The cold-bursting efficiency is controlled by the water penetration into the lipid particle which, in turn, is related to the size of crystalline domains and the number density of nanopores formed between these domains. For that reason, most efficient cold-bursting for pure TAGs was observed after *rapid cooling* [40].

Similar trends were observed with the triglyceride mixtures in the current study. Most efficient particle disintegration was observed with *rapidly cooled* emulsions, which were then *slowly heated*, see Fig. 6a and Supplementary Movie 4. The initial *M2a* particles with average diameter of *ca.* 45 μm, dispersed in C_{12}SorbEO$_{20}$ + $C_{16–18}$MG solution, disintegrated spontaneously into sub-micrometer droplets with diameter ≈ 420 ± 65 nm (measured by volume) after one cooling-heating cycle only. After several cooling-heating cycles, the average particle size decreased down to 20 nm. With *M6* mixture, studied under equivalent conditions, we also observed significant drop size decrease, however, bigger drops also remained in the latter sample even after five consecutive cooling-heating cycles. When we combined C_{12}SorbEO$_{20}$ surfactant with $C_{18:1}$MG instead of $C_{16–18}$MG, we observed complete particle disintegration down to particle diameter d_{32} ≈ 20 nm when using *rapid cooling* and *slow heating*, even with *M6* TAG mixture, see Fig. 7.

The disintegration efficiency for *M2a* drops dispersed in C_{12}SorbEO$_{20}$ + $C_{16–18}$MG surfactant solution was significantly decreased when the same sample was *rapidly cooled* and then *heated fast*, Fig. 6b. In this case, the obtained drops were of micrometer size and many drops with diameter around 25 μm remained. These results emphasize the role of the time available for the aqueous phase to penetrate into the lipid particles and to disintegrate them. In some oil-surfactant systems, double W/O/W emulsion drops were formed when this temperature protocol was applied (the respective mechanism is explained below when discussing the *slow cooling-fast heating* protocol).

When this experiment was performed with *slow cooling* and *slow heating* rates, we observed the formation of numerous smaller micrometer drops, while the main fraction of the oil remained included inside the original oily drops, Fig. 6c. Slow cooling rates favor the formation of smaller in number and bigger in size crystalline domains. Hence, although the aqueous phase has enough time to infuse the lipid particles, the number of nanopores between the crystal domains is limited and the disintegration is less efficient than in the rapidly cooled systems.

In the emulsions subjected to *slow cooling-fast heating* cycle, we observed the formation of W/O/W emulsion drops, see Figs. 6d and 8, and Supplementary Movie 5. The melting temperature interval of some of the TAG mixtures spans the heating process: for *M6* the melting process starts at sub-zero temperatures with the melting of tricaprin

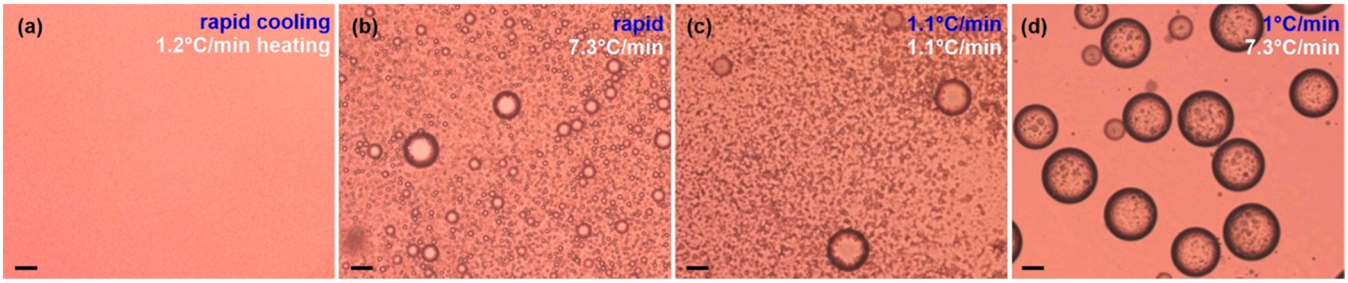

Fig. 6. Effect of the cooling-heating protocol. **(a)** Complete drop disintegration is observed upon *rapid cooling* and subsequent *slow heating*, see also Supplementary Movie 4. **(b,c)** The bursting process is less efficient in the case of *rapid cooling* and *fast heating* or (b) when *slow cooling* and *heating* (c) is applied. **(d)** Double W/O/W emulsion droplets form upon *slow cooling* and subsequent *fast heating*, see also Supplementary Movie 5. The studied system is *M2a* drops, dispersed in $C_{12}SorbEO_{20}$ + $C_{16-18}MG$, initial drop size ≈ 45 μm. Scale bars = 20 μm.

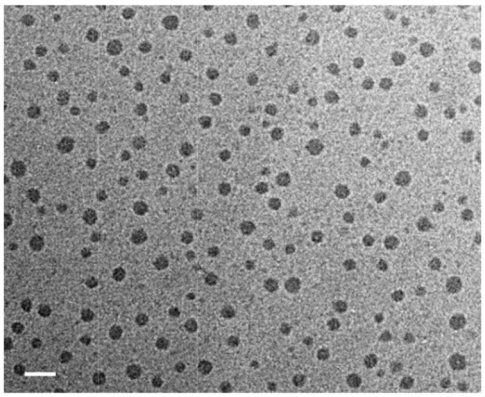

Fig. 7. Cryo-TEM image of *M6* nanoparticles dispersed in $C_{12}SorbEO_{20}$ + $C_{18:1}MG$ surfactant solution. The average particle size is ≈ 20 nm. Sample with 1 wt% oil has been used. These nanoparticles are prepared from a course oil-in-water emulsion (d ≈ 50 μm) which was cooled and heated in five consecutive cycles, with cooling rate ≈ 5 °C/min and heating rate ≈ 1.5 °C/min. Scale bar = 50 nm.

(C_8TAG) and continues up to *ca.* 53 °C until tripalmitin ($C_{16}TAG$) melts. For that reason, the penetrating water may become surrounded by molten oil – instead of disrupting the solid-liquid structure, water remains trapped inside the melting particles, Fig. 8.

We note that the initial emulsion is exactly the same in these experiments, Fig. 6. Therefore, the observed different types of behavior are entirely due to kinetic effects. When the aqueous phase penetrates into the lipid particle, it needs finite time to wet the lipid crystalline domains and to induce their separation. When this time is insufficient, the water gets trapped inside the melting oily drops to form W/O/W at the end of the melting process, Fig. 8. The size of the entrapped water droplets varied between *ca.* 1 and 20 μm. It depended primarily on the heating protocol, the concentration of oil-soluble surfactant (which stabilizes the newly formed water droplets against coalescence) and the size of the oily drops in which the water droplets are entrapped. Higher in number and smaller in size water droplets were entrapped when the frozen mixed TAG particles were heated at higher heating rates in samples containing oil-soluble surfactant of higher concentration, see Fig. 9e. At lower cooling rates and/or at low concentration of the oil-soluble surfactant, the infused water pockets coalesced with each other and formed bigger in size and lower in number water droplets, see Fig. 9a,b,d.

The discussed switch between cold-bursting and double emulsion formation was observed with numerous TAG mixtures, see Supplementary Table S1. Note that, for a single-component TAG systems with given chemical composition, such switch was not observed by changing the heating rate only. For a given single-component TAG system, one can change the behavior from particle disintegration to double emulsion formation or *vice versa* only by changing the surfactants present in the system, which control the wetting properties of the surfactant solution.

3.3.2. *Oil-soluble surfactant - concentration and phase for initial dissolution*

The concentration of the oil-soluble surfactant in the aqueous phase controls the wetting properties of the surfactant solution over the TAG solid surface. The contact angle decreases significantly when the concentration of oil-soluble surfactant is increased. Therefore, by changing the concentration of oil-soluble surfactant we can change also the behavior of the emulsified TAG mixtures. Example for this type of control is presented in Fig. 9. Double W/O/W emulsion drops form after one cooling-heating cycle when *M2a* drops are dispersed in 1.5 wt% $C_{12}SorbEO_{20}$ solution, Figs. 9a and 9e. The addition of 0.1 wt% $C_{18:1}EO_2$ into the aqueous phase suppressed the double emulsion formation significantly (Fig. 9b), whereas the increase of the oil-soluble surfactant concentration to 0.5 wt% led to complete particle bursting after one

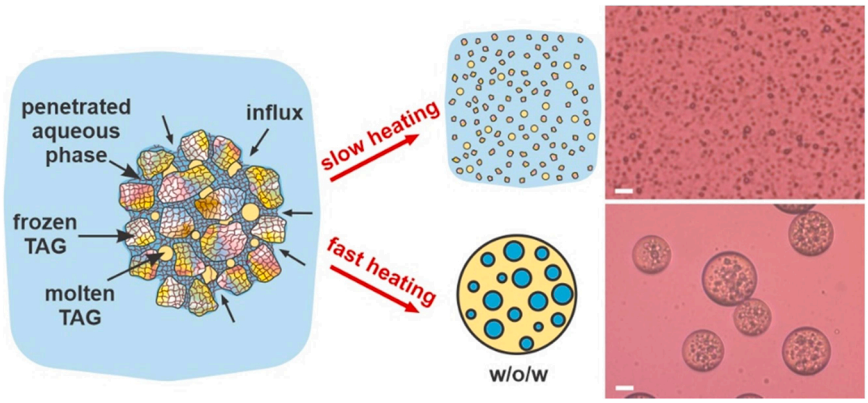

Fig. 8. Schematic presentation of the competition between particle bursting and W/O/W drop formation depending on heating rate. Upon heating, the multicomponent TAG particles contain already molten TAG, still frozen TAG domains, and penetrated aqueous phase. Depending on the heating rate, the penetrated aqueous phase may become trapped inside the melting lipid globule, thus forming double emulsion droplets of type W/O/W (when *fast heating* is applied). Alternatively, upon *slow heating*, the initial lipid particle can disintegrate into millions of nanoparticles. Scale bars on the microscopy images = 20 μm.

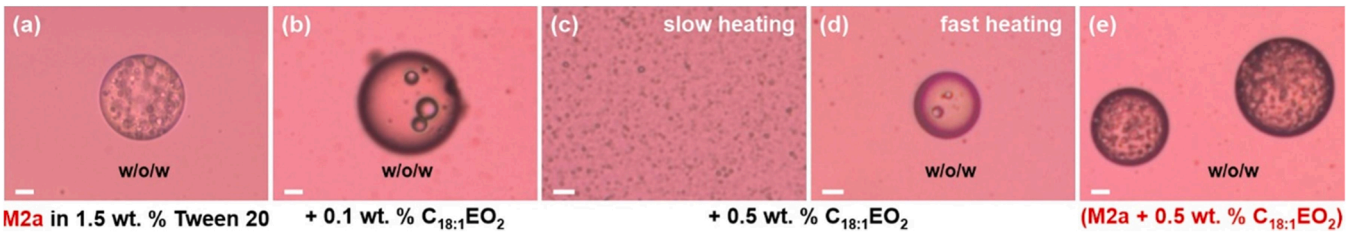

Fig. 9. Control over the cold-bursting and double emulsion formation processes. Optical microscopy images illustrating the typical behavior of samples after *rapid cooling* and subsequent *slow heating*, except for (d) where *fast heating* was applied. All samples are prepared with *M2a* mixture, dispersed in 1.5 wt% $C_{12}SorbEO_{20}$ solution in the absence or in the presence of $C_{18:1}EO_2$ surfactant, dissolved either in the aqueous or in the oily phase. (a) *M2a* in 1.5 wt% $C_{12}SorbEO_{20}$; (b) *M2a* in (1.5 wt% $C_{12}SorbEO_{20}$ + 0.1 wt% $C_{18:1}EO_2$) solution; (c-d) *M2a* in (1.5 wt% $C_{12}SorbEO_{20}$ + 0.5 wt% $C_{18:1}EO_2$) solution; (e) (*M2a* + 0.5 wt% $C_{18:1}EO_2$) in 1.5 wt% $C_{12}SorbEO_{20}$. Heating rate: 0.9 °C/min for (a-c,e) and 4.5 °C/min for (d). Scale bar = 10 μm.

cooling-heating cycle only when *slow heating* was applied, see Fig. 9c. This type of emulsion control relies on the selection of appropriate TAG-surfactant combinations and it is applicable to pure triglycerides as well [40]. As explained already, the temperature protocol has a major effect on the observed processes. If the *M2a* drops dispersed in 1.5 wt% $C_{12}SorbEO_{20}$ + 0.5 wt% $C_{18:1}EO_2$ are heated with higher rate after *rapid cooling*, we observed the formation of W/O/W drops, see Fig. 9d.

All results described to this point were obtained with emulsions in which the oil-soluble surfactant had been always added into the aqueous phase. As explained above, we use this procedure, because the incorporation of the oil-soluble surfactant in the micelles of the water-soluble surfactant leads to the formation of large supramolecular aggregates. These aggregates are very efficient to create osmotic pressure difference between the external and internal aqueous phase, see Fig. 1d for illustration, thus boosting the cold-bursting process. Alternatively, when the oil-soluble surfactant is pre-dissolved in the oily phase, such osmotic pressure gradient is missing and the behavior of the system is governed predominantly by the wetting properties of the aqueous phase. For example, *M2a* drops dispersed in $C_{12}SorbEO_{20}$ solution formed double W/O/W drops in the absence of oil-soluble surfactant or when the latter is pre-dissolved in the oily phase, see Figs. 9a and 9e. The particles did not disintegrate even when up to 10 wt% oil-soluble surfactant ($C_{18:1}EO_2$ or $C_{18:1}MG$) was pre-dissolved in *M2* or *M6* triglyceride mixtures (the aqueous solution contained only the water-soluble $C_{12}SorbEO_{20}$), see Supplementary Figure S8. For comparison, *M2* particles disintegrated when the aqueous solution contained as little as 0.5 wt% of oil-soluble surfactant, highlighting its importance in inducing the osmotic pressure.

3.3.3. Initial drop size

The cold-bursting and double emulsion formation are affected also by the initial drop size which determines the amount of aqueous phase needed to infuse the frozen lipid particle and the time period required for this infusion. Larger in number and bigger in size water droplets are entrapped inside the molten triglyceride drops when they are larger than *ca.* 30 μm, whereas more efficient cold-bursting is observed with the smaller initial particles.

The initial drop size may even determine the particle behavior for systems in which the bursting efficiency is relatively low, *viz.* there is limited disintegration from particles' surface only. For example, *M6* drops with sizes up to *ca.* 30 μm undergo partial cold-bursting and decrease their size upon cooling and heating, when dispersed in 1.5 wt% $C_{12}SorbEO_{20}$ + 0.5 wt% $C_{18:1}EO_2$ solution. In contrast, bigger initial drops (≳ 35 μm) entrapped water and formed double emulsion drops in the same surfactant solution, using the same thermal protocol. Illustrative images of this behavior are presented in Supplementary Figure S9.

4. Conclusions

We studied the processes of cold-bursting and double emulsion formation with oily drops composed of monoacid TAG mixtures. We show that the cold-bursting efficiency decreases with the complexity of the mixture composition. Nevertheless, complete bursting into nanoparticles is possible even for the most complex TAG mixtures under optimized conditions. The smallest particle size that we achieved by cooling and heating was ≈ 20 nm for all TAG mixtures studied, including the most complex six-component TAG mixture.

Key requirements for efficient cold-bursting are: (1) the aqueous surfactant solution should contain large supramolecular aggregates which are able to create osmotic pressure difference during the infusion of the aqueous phase into the nanopore structure, Fig. 1; (2) the oil-soluble surfactant should crystallize separately from the TAG molecules upon cooling (*viz.* to phase separate) which allows the formation of more hydrophilic domains, thus improving the aqueous phase infusion; and (3) If the surfactant melts at lower temperature compared to TAGs upon heating, the cold-bursting efficiency is additionally improved due to pore swelling by the melting MG. Such type of behavior was observed with glycerol monooleate which satisfies all requirements and it is an excellent booster of the cold-bursting process.

The wide temperature interval for melting of TAG mixtures allowed us to switch between cold-bursting and double W/O/W emulsion formation for systems with the same chemical composition, by changing the temperature protocol only. Most efficient bursting was observed when *rapid cooling-slow heating* protocol was used, whereas the *slow cooling-fast heating* protocol led to the formation of double W/O/W emulsions, because the penetrating water became trapped inside the quickly melting TAG particles. Variations in the concentration of the oil-soluble surfactant added to the aqueous phase could be also used for process control, because it changes the osmotic effect and the wetting ability of the surfactant solution in contact with the frozen lipid.

The main conclusions from the current study can be used as guiding principles for preparation of nanometer sized particles and double emulsions from mixed triglycerides – systems of definite interest in several applied areas and technologies, *e.g.* in pharmaceutical and theragnostic products, cosmetics, foods and soft matter materials.

CRediT authorship contribution statement

Diana Cholakova: Conceptualization, Methodology, Investigation, Validation, Formal analysis, Visualization, Writing – original draft, Writing – review & editing, Project administration. **Desislava Glushkova:** Investigation, Visualization, Formal analysis, **Martin Pantov:** Investigation, Visualization, Formal analysis. **Slavka Tcholakova:** Conceptualization, Supervision, Writing – review & editing, Funding acquisition. **Nikolai Denkov:** Conceptualization, Supervision, Writing – review & editing, Funding acquisition.

Declaration of Competing Interest

The authors declare that they have no known competing financial interests or personal relationships that could have appeared to influence the work reported in this paper.

Data availability

Data will be made available on request.

Acknowledgements

The study was funded by Bulgarian Ministry of Education and Science, under the National Research Program "VIHREN", project ROTA-Active (no. KP-06-DV-4/16.12.2019). The authors acknowledge the possibility to use SAXS/WAXS instrument purchased for execution of project BG05M2OP001–1.002-0012 and the possibility to use DSA 100E, purchased for execution of project BG05M2OP001–1.001–0008, Operational Program "Science and Education for Smart Growth", Bulgaria. The authors are grateful to Mrs. K. Rusanova and Dr. L. Mihaylov (Sofia University) for cryo-TEM imaging and to Dr. M. Boneva-Astrukova (Sofia University) for performing part of the three-phase contact angle measurements.

Appendix A. Supporting information

Supplementary data associated with this article can be found in the online version at doi:10.1016/j.colsurfa.2023.131439.

References

[1] L. Hodson, C.M. Skeaff, B.A. Fielding, Fatty acid composition of adipose tissue and blood in humans and its use as a biomarker of dietary intake, Prog. Lipid Res. 47 (2008) 348–380, https://doi.org/10.1016/j.plipres.2008.03.003.
[2] R. Singh, S. Kaushik, Y. Wang, Y. Xiang, I. Novak, M. Komatsu, K. Tanaka, A. M. Cuervo, M.J. Czaja, Autography regulates lipid metabolism, Nature 458 (2009) 1131–1135, https://doi.org/10.1038/nature07976.
[3] Y. Yang, D.J. McClements, Encapsulation of vitamin E in edible emulsions fabricated using a natural surfactant, Food Hydrocoll. 30 (2013) 712–720, https://doi.org/10.1016/j.foodhyd.2012.09.003.
[4] X. Liu, R. Zhang, D.J. McClements, F. Li, H. Liu, Y. Cao, H. Xiao, Nanoemulsion-based delivery systems for nutraceuticals: influence of long-chain triglyceride (LCT) type on in vitro digestion and astaxanthin bioaccessibility, Food Biophys. 13 (2018) 412–421, https://doi.org/10.1007/s11483-018-9547-2.
[5] L. Salvia-Trujillo, D.J. McClements, Improvement of β-carotene bioaccessibility from dietary supplements using excipient nanoemulsions, J. Agric. Food Chem. 64 (2016) 4639–4647, https://doi.org/10.1021/acs.jafc.6b00804.
[6] A. Gupta, H.B. Eral, T.A. Hatton, P.S. Doyle, Nanoemulsions: Formation, properties and applications, Soft Matter 12 (2016) 2826–2841, https://doi.org/10.1039/c5sm02958a.
[7] R.H. Müller, R.D. Petersen, A. Hommoss, J. Pardeike, Nanostructured lipid carriers (NLC) in cosmetic dermal products, Adv. Drug Deliv. Rev. 59 (2007) 522–530, https://doi.org/10.1016/j.addr.2007.04.012.
[8] C. Dima, E. Assadpour, S. Dima, S.M. Jafari, Bioactive-loaded nanocarriers for functional foods: from designing to bioavailability, Curr. Opin. Food Sci. 33 (2020) 21–29, https://doi.org/10.1016/j.cofs.2019.11.006.
[9] E. Rostami, S. Kashanian, A.H. Azandaryani, H. Faramarzi, J.E.N. Dolatabadi, K. Omidfar, Drug targeting using solid lipid nanoparticles, Chem. Phys. Lipids 181 (2014) 56–61, https://doi.org/10.1016/j.chemphyslip.2014.03.006.
[10] W. Dai, C. Ruan, Y. Zhang, J. Wang, J. Han, Z. Shao, Y. Sun, J. Liang, Bioavailability enhancement of EGCG by structural modification and nano-delivery: a Review, J. Funct. Foods 65 (2020), 103732, https://doi.org/10.1016/j.jff.2019.103732.
[11] D.J. McClements, J. Rao, Food-grade nanoemulsions: formulation fabrication properties performance biological fate and potential toxicity, Crit. Rev. Food Sci. Nutr. 51 (2011) 285–330, https://doi.org/10.1080/10408398.2011.559558.
[12] W. Mehnert, K. Mäder, Solid lipid nanoparticles. Production Characterization and Applications, in: Adv. Drug Delivery Rev., 2001, pp. 165–196, https://doi.org/10.1016/s0169-409x(01)00105-3.
[13] C. Qian, E.A. Decker, H. Xiao, D.J. McClements, Solid lipid nanoparticles: effect of carrier oil and emulsifier type on phase behavior and physical stability, J. Am. Oil Chem. Soc. 89 (2012) 17–28, https://doi.org/10.1007/s11746-011-1882-0.
[14] A. Kumar, R. Kaur, V. Kumar, S. Kumar, R. Gehlot, P. Aggarwal, New insights into water-in-oil-in-water (w/o/w) double emulsions: properties fabrication instability mechanism and food applications, Trends Food Sci. Technol. 128 (2022) 22–37, https://doi.org/10.1016/j.tifs2022.07.016.
[15] B.S.T. Barbosa, E.E. Garcia-Rojas, Double emulsions as delivery systems for iron: Stability kinetics and improved bioaccessibility in infants and adults, Curr. Res. Food Sci. 5 (2022) 718–725, https://doi.org/10.1016/j.crfs.2022.04.003.
[16] M.-J. Choi, D. Choi, J. Lee, Y.-J. Jo, Encapsulation of a bioactive peptide in a formulation of W1/O/W2-type double emulsions: formation and stability, Food Struct. 25 (2020), 100145, https://doi.org/10.1016/j.foostr.2020.100145.
[17] M. Bonnet, M. Cansell, A. Berkaoui, M.H. Ropers, M. Anton, F. Leal-Calderon, Release rate profiles of magnesium from multiple w/o/w emulsions, Food Hydrocoll. 23 (2009) 92–101, https://doi.org/10.1016/j.foodhyd.2007.11.016.
[18] Y.H. Choi, J. Hwang, S.H. Han, C. Lee, S. Jeon, S. Kim, Thermo-responsive microcapsules with tunable molecular permeability for controlled encapsulation and release, Adv. Funct. Mater. 31 (2021) 2100782, https://doi.org/10.1002/adfm.202100782.
[19] C. Dima, S. Dima, Bioaccessibility study of calcium and vitamin D3 co-microencapsulated in water-in-oil-in-water double emulsions, Food Chem. 303 (2020), 125416, https://doi.org/10.1016/j.foodchem.2019.125416.
[20] J. Liu, M. Kharat, Y. Tan, H. Zhou, J.L.M. Mundo, D.J. McClements, Impact of fat crystallization on the resistance of w/o/w emulsions to osmotic stress: potential for temperature-triggered release, Food Res. Int. 134 (2020), 109273, https://doi.org/10.1016/j.foodres.2020.109273.
[21] H.J. Giroux, S. Constantineau, P. Fustier, C.P. Champagne, D. St-Gelais, M. Lacroix, M. Britten, Cheese fortification using water-in-oil-in-water double emulsions as carrier for water soluble nutrients, Int. Dairy J. 29 (2013) 107–114, https://doi.org/10.1016/j.idairyj.2012.10.009.
[22] V. Nelis, A. Declerck, L. De Neve, K. Moens, K. Dewettinck, P. Van der Meeren, Fat crystallization and melting in w/o/w double emulsions: comparison between bulk and emulsified state, Colloids Surf. A 566 (2019) 196–206, https://doi.org/10.1016/j.colsurfa.2019.01.019.
[23] H. Xu, Y. Niu, W. Hong, W. Liu, X. Zuo, X. Bao, C. Guo, Y. Lu, B. Deng, Development of a water-in-oil-in-water adjuvant for foot-and-mouth disease vaccine based on ginseng stem-leaf saponins as an immune booster, Comp. Immunol. Microbiol. Infect. Dis. 71 (2020), 101499, https://doi.org/10.1016/j.cimid.2020.101499.
[24] H.J. Yang, I.S. Park, K. Na, Biocompatible microspheres based on acetylated polysaccharide prepared from water-in-oil-in-water (w1/o/w2) double-emulsion method for delivery of type II diabetic drug (exenatide), Colloids Surf. A 340 (2009) 115–120, https://doi.org/10.1016/j.colsurfa.2009.03.015.
[25] C.-X. Zhao, D. Chen, Y. Hui, D.A. Weitz, A.P.J. Middelberg, Stable ultrathin-shell double emulsions for controlled release, ChemPhysChem 17 (2016) 1553–1556, https://doi.org/10.1002/cphc.201600142.
[26] K. Pays, J. Giermanska-Kahn, B. Puligny, J. Bibette, F. Leal-Calderon, Double emulsions: how does release occur? J. Control. Release 79 (2002) 193–205, https://doi.org/10.1016/S0168-3659(01)00535-1.
[27] J. Andrade, A.J. Wright, M. Corredig, In vitro digestion behavior of water-in-oil-in-water emulsions with gelled oil-water inner phases, Food Res. Int. 105 (2018) 41–51, https://doi.org/10.1016/j.foodres.2017.10.070.
[28] W. Li, W. Wang, C. Yong, Y. Lan, Q. Huang, J. Xiao, Effects of the distribution site of crystallizable emulsifiers on the gastrointestinal digestion behavior of double emulsions, J. Agric. Food Chem. 70 (2022) 5115–5125, https://doi.org/10.1021/acs.jafc.1c07987.
[29] B. Zheng, X. Li, J. Hao, D. Xu, Meat systems produced with Monascus pigment water-in-oil-in-water multiple emulsion as pork fat replacers, Food Chem. 402 (2023), 134080, https://doi.org/10.1016/j.foodchem.2022.134080.
[30] R.C. Chevalier, A. Gomes, R.L. Cunha, Role of aqueous phase composition and hydrophilic emulsifier type on the stability of w/o/w emulsions, Food Res. Int. 156 (2022), 111123, https://doi.org/10.1016/j.jfoodres.2022.111123.
[31] G. Muschiolik, E. Dickinson, Double emulsions relevant to food systems: preparation stability and applications, Compr. Rev. Food Sci. Food Saf. 16 (2017) 532–555, https://doi.org/10.1111/1541-4337.12261.
[32] L. Sapei, M.A. Naqvi, D. Rousseau, Stability and release properties of double emulsions for food applications, Food Hydrocoll. 27 (2012) 316–323, https://doi.org/10.1016/j.foodhyd.2011.10.008.
[33] N. Chiu, L. Hewson, I. Fisk, B. Wolf, Programmed emulsions for sodium reduction in emulsion based foods, Food Funct. 6 (2015) 1428–1434, https://doi.org/10.1039/C5FO00079C.
[34] A.S. Utada, E. Lorenceau, D.R. Link, P.D. Kaplan, H.A. Stone, D.A. Weitz, Monodisperse double emulsions generated from a microcapillary device, Science 308 (2005) 537–541, https://doi.org/10.1126/science.1109164.
[35] L.-Y. Chu, A.S. Utada, R.K. Shah, J.-W. Kim, D.A. Weitz, Controllable monodisperse multiple emulsions, Angew. Chem. Int. Ed. 46 (2007) 8970–8974, https://doi.org/10.1002/anie.200701358.
[36] V. Nelis, A. Declerck, L. Vermeir, M. Balcaen, K. Dewettinck, P. Van der Meeren, Fat crystals: a tool to inhibit molecular transport in w/o/w double emulsions, Magn. Reson. Chem. 57 (2019) 707–718, https://doi.org/10.1002/mrc.4840.
[37] J. Guery, J. Baudry, D.A. Weitz, P.M. Chaikin, J. Bibette, Diffusion through colloidal shells under stress (R), Phys. Rev. E 79 (2009), 060402, https://doi.org/10.1103/PhysRevE.79.060402.
[38] S. Frasch-Melnik, F. Spyropoulos, I.T. Norton, $W_1/O/W_2$ double emulsions stabilized by fat crystals - formulation stability and salt release, J. Colloid Interface Sci. 350 (2010) 178–185, https://doi.org/10.1016/j.jcis.2010.06.039.
[39] E. Tenorio-Garcia, A. Araiza-Calahorra, E. Simone, A. Sarkar, Recent advances in design and stability of double emulsions: trends in Pickering stabilization, Food Hydrocoll. 128 (2022), 107601, https://doi.org/10.1016/j.foodhyd.2022.107601.
[40] D. Cholakova, D. Glushkova, S. Tcholakova, N. Denkov, Nanopore and nanoparticles formation with lipids undergoing polymorphic phase transitions, ACS Nano 14 (2020) 8594–8604, https://doi.org/10.1021/acsnano.0c02946.
[41] D. Cholakova, D. Glushkova, S. Tcholakova, N. Denkov, Cold-burst method for nanoparticle formation with natural triglyceride oils, Langmuir 37 (2021) 7875–7889, https://doi.org/10.1021/acs.langmuir.0c02967.
[42] I. Lesov, D. Glushkova, D. Cholakova, M.T. Georgiev, S. Tcholakova, S.K. Smoukov, N. Denkov, Flow reactor for preparation of lipid nanoparticles via temperature

variations, J. Ind. Eng. Chem. 112 (2022) 37–45, https://doi.org/10.1016/j.jiec.2022.03.043.
[43] D.M. Small, The Physical Chemistry of Lipids. From Alkanes to phospholipids in Handbook of Lipid Research, Plenum,, New York, 1986.
[44] K. Sato, Crystallization of lipids: Fundamentals and applications in food, cosmetics and pharmaceuticals, Wiley Blackwell,, 2018, https://doi.org/10.1002/9781118593882.
[45] N. Arita-Merino, H. van Valenberg, E.P. Gilbert, E. Scholten, Quantitative phase analysis of complex fats during crystallization, Cryst. Growth Des. 20 (2020) 5193–5202, https://doi.org/10.1021/acs.cgd.0c00416.
[46] H. Bunjes, K. Westesen, M.H.J. Koch, Crystallization tendency and polymorphic transitions in triglyceride nanoparticles, Int. J. Pharm. 129 (1996) 159–173, https://doi.org/10.1016/0378-5173(95)04286-5.
[47] D.J. Cebula, D.J. McClements, M.J.W. Povey, Small angle neutron scattering from voids in crystalline trilaurin, J. Am. Oil Chem. Soc. 67 (1990) 76–78, https://doi.org/10.1007/BF02540630.
[48] S. Sonwai, P. Rungprasertphol, N. Nantipipat, S. Tungvongchatoan, N. Laiyangkoon, Characterization of coconut oil fractions obtained from solvent fractionation using acetone, J. Oleo Sci. 66 (2017) 951–961, https://doi.org/10.5650/jos.ess16224.
[49] E. Koukoura, M. Panagiotopoulou, A. Pavlou, V. Karageorgiou, D.G. Fatouros, C. Vasiliadou, C. Ritzoulis, In vitro digestion of caseinate and Tween 20 emulsions, Food Biophys. 14 (2019) 60–68, https://doi.org/10.1007/s11483-018-9557-0.
[50] L. Perugini, G. Cinelli, M. Cofelice, A. Ceglie, F. Lopez, F. Cuomo, Effect of the coexistence of sodium caseinate and Tween 20 as stabilizers of food emulsions at acidic pH, Colloids Surf. B 168 (2018) 163–168, https://doi.org/10.1016/j.colsurfb.2018.02.003.
[51] Y.-K. Oh, M.Y. Kim, J.-Y. Shin, T.W. Kim, M.-O. Yun, S.J. Yang, S.S. Choi, W.-W. Jung, J.A. Kim, H.-G. Choi, Skin permeation of retinol in Tween 20-based deformable liposomes: in-vitro evaluation in human skin and keratinocyte models, J. Pharm. Pharmacol. 58 (2006) 161–166, https://doi.org/10.1211/jpp.58.2.0002.
[52] R.B. Chavan, S.R. Modi, A.K. Bansal, Role of solid carriers in pharmaceutical performance of solid supersaturable SEDDS of celecoxib, Int. J. Pharm. 495 (2015) 374–384, https://doi.org/10.1016/j.ijpharm.2015.09.011.
[53] D. Cholakova, N. Denkov, S. Tcholakova, Z. Valkova, S.K. Smoukov, Multilayer formation in self-shaping emulsion droplets, Langmuir 35 (2019) 5484–5495, https://doi.org/10.1021/acs.langmuir.8b02771.
[54] D. Cholakova, S. Tcholakova, N. Denkov, Polymorphic phase transitions in bulk triglyceride mixtures, Cryst. Growth Des. 23 (2023) 2075–2091, https://doi.org/10.1021/acs.cgd.2c01021.
[55] I. Niiya, T. Maruyama, M. Imamura, M. Okada, T. Matsumoto, T. Matsumoto, Effect of emulsifiers on the crystal growth of edible solid fats. part III. effect of saturated fatty acid monoglyceride, Nippon Shokuhin Kogyo Gakkaishi 20 (1973) 182–190, https://doi.org/10.3136/nskkk1962.20.182.
[56] C. Lopez, M. Ollivon, Crystallisation of triacylglycerols in nanoparticles, J. Therm. Anal. Calor. 98 (2009) 29–37, https://doi.org/10.1007/s10973-009-0183-4.
[57] A. Alfutimie, N. Al-Janabi, R. Curtis, G.J.T. Tiddy, The effect of monoglycerides on the crystallisation of triglyceride, Colloids Surf. A 494 (2016) 170–179, https://doi.org/10.1016/j.colsurfa.2016.01.029.
[58] D. Cholakova, D. Glushkova, Z. Valkova, S. Tsibranska-Gyoreva, K. Tsvetkova, S. Tcholakova, N. Denkov, Rotator phases in hexadecane emulsion drops revealed by X-ray synchrotron techniques, J. Colloid Interface Sci. 604 (2021) 260–271, https://doi.org/10.1016/j.jcis.2021.06.122.
[59] G. Rizzo, J.E. Norton, I.T. Norton, Emulsifier effects on fat crystallization, Food Struct. 4 (2015) 27–33, https://doi.org/10.1016/j.foostr.2014.11.002.